Fundamental-mode laser-beam propagation in optically inhomogeneous electrochemical media with chemical species concentration gradients

Andreas Mandelis and Barrie S. H. Royce

Solutions to Maxwell's wave equation have been derived for the propagation of the fundamental (Gaussian) mode of a laser beam in a fluid electrolyte which is in contact with an active electrode. An electrochemical or photoelectrochemical reaction at the electrolyte–electrode interface is assumed to generate a concentration gradient of the product in the electrolyte, which results in an inhomogeneous refractive-index profile. The analytic solutions for the propagation of the beam explicitly demonstrate the dependence of the displacement of the intensity centroid and of the spot shape on the electrochemical parameters of the system.

I. Introduction

Reactions taking place at an electrode–electrolyte interface in a electrochemical or photoelectrochemical environment are of considerable fundamental and technological interest. Such reactions are pertinent to the problem of corrosion, the design of fuel cells and photoelectrochemical cells for solar energy conversion, electrochemical reactors for product synthesis, and species specific electrodes for chemical analysis. Semiconducting electrodes are an important subset of those available for these applications, and the semiconductor band structure plays an essential role in the electrode stability, charge transfer to electrolyte species, and the interaction with incident radiation. These processes can be influenced by the chemical species present on the electrode surface and thus may be used to obtain insight into the basic charge transfer mechanisms occurring at the semiconductor–electrolyte interface with a case of particular interest being a semiconducting electrode undergoing competitive interfacial charge transfer and photodecomposition reactions. A fundamental understanding of such processes is essential for the fabrication of stable photoelectrodes and electrocatalytic surfaces that are species specific as well as for control of fuel cell behavior.

Mechanisms of interfacial charge transfer at semiconducting and oxidized metal interfaces have been subject to a wide variety of studies and are discussed in books by Bard and Faulkner,[1] Bockris and Kahn,[2] and Morrison.[3] However, relatively little data are available on the actual surface processes involved. Conventional electrochemical and photoelectrochemical methods can be employed to provide some mechanistic and thermodynamic information; however, it is highly desirable to be able to combine these methods with species specific probes, such as spectroscopy, so that competitive reactions involving multiple species may be deconvoluted. Utilization of a spectroscopic probe further allows the monitoring of nonelectroactive species which may play a role in the interfacial charge transfer process.

Charge transfer processes to solution species and the electrode dissolution processes that may occur in electrochemical and photoelectrochemical systems generate time-dependent species concentrations in the region of the electrode–electrolyte interface. Recently, these species gradients have been probed experimentally[4–6] using the mirage effect [or photothermal deflection spectroscopy (PDS)].[7,8] In these experimental studies the displacement of the intensity centroid of a laser beam propagating parallel to the electrode–electrolyte interface is used to obtain spectroscopic or species concentration information. A theoretical model appropriate to the spectroscopic studies has been developed by Mandelis.[9]

In addition to experiencing an intensity centroid displacement due to the near-electrode refractive-index gradient, the laser beam undergoes a shape change since

Andreas Mandelis is with University of Toronto, Department of Mechanical Engineering, Photoacoustics Laboratory, Toronto, Ontario M5S 1A4, and B. S. H. Royce is with Princeton University, Applied Physics & Materials Laboratory, Princeton, New Jersey 08544.

Received 5 April 1984.
0003-6935/84/172892-10$02.00/0.

light propagating close to the interface samples a higher spatial gradient than that propagating farther away from the interface.

This paper examines the problem of laser beam propagation in electrochemical media with a refractive-index gradient due to inhomogeneous chemical species concentration distributions. Analytical solutions to the wave equation governing the electromagnetic field of the propagating light beam have been obtained for media having slow spatial variations of the index of refraction. These solutions are rigorously valid for laser beam propagation in a fluid electrolyte in contact with an electrode surface. The laser beam intensity centroid is assumed to be parallel and adjacent to the electrode surface which is kept at a constant concentration of an electrochemical species at all times after initiation of the reaction, while electrolyte diffusion processes generate a concentration gradient in the fluid.

II. Diffusion Problem: Refractive-Index Profile

The system geometry is shown in Fig. 1. For an isothermal electrochemical system which contains a semi-infinite electrode in contact with a fluid electrolyte, the concentration profile of a chemical species produced at the interface is given by[10]

$$C(x,t) = C_0 \operatorname{erfc}\left(\frac{x}{2\sqrt{Dt}}\right) \tag{1}$$

for the geometry of Fig. 1, where C_0 is the concentration of the product chemical species on the electrode surface and is assumed constant at all times, and D is the diffusion coefficient (cm^2-sec^{-1}) of the particular chemical species in the electrolyte.

The concentration profile $C(x,t)$ described in Eq. (1) induces a refractive-index gradient in the electrolyte, which, for small departures from uniformity, can be expressed in terms of a Taylor series expansion around the value of the refractive index n_0 of the electrolyte when $C = 0$:

$$n(x,t) \cong n_0 + C_0\left(\frac{\partial n}{\partial C}\right)_{C=C_0} \operatorname{erfc}\left(\frac{x}{2\sqrt{Dt}}\right), \tag{2}$$

where only first-order terms were kept, since

$$C_0\left(\frac{\partial n}{\partial C}\right)_{C=C_0} \ll 1$$

for many systems of practical interest [e.g., $C_0(\partial n/\partial C)_{C=C_0} = 5.9 \times 10^{-3}$ for an aqueous solution of $CuSO_4$ at 20°C with a surface concentration $C_0 = 0.2$ moles/liter[11,12]; for aqueous solutions of H_2SO_4 at 20°C below 10 M, $C_0(\partial n/\partial C)_{C=C_0} \leq 8 \times 10^{-3}$ for a surface concentration $C_0 = 1$ M[11,12]].

III. Optical Propagation Problem: Solution to Maxwell's Equations in the Index Profile of Eq. (2)

The general solution to Maxwell's equations for the electric and magnetic fields propagating along a laser beam axis can be simplified considerably without loss of generality by considering a polarized beam which has no electric field component in the y direction or magnetic field component in the x direction with the coordinates as specified in Fig. 1. The remaining field components yield identical equations for e_x and h_y. For e_x in the fluid electrolyte medium[13]

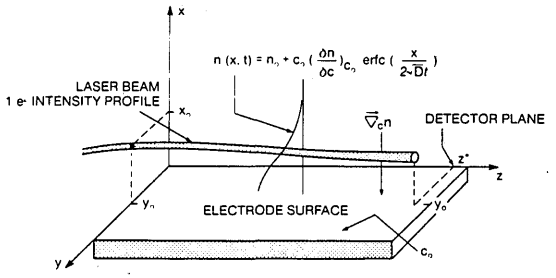

Fig. 1. Schematic diagram of laser beam propagation in electrochemical medium near the electrode–electrolyte interface in the presence of a refractive-index gradient $\nabla_c n$ due to an electrochemical species concentration gradient: C_0, species concentration at electrode surface; D, species diffusion coefficient in the electrolyte; n_0, refractive index of the electrolyte in the absence of a concentration gradient.

$$\nabla^2 e_x(x,y,z;t) - \mu_0\left[\varepsilon(x,t)\frac{\partial^2}{\partial t^2}e_x(x,y,z;t) + \frac{\partial}{\partial t}\varepsilon(x,t)\frac{\partial}{\partial t}e_x(x,y,z;t)\right] = 0, \tag{3}$$

where the magnetic permeability μ of the medium was taken to be that of a vacuum, $\mu = \mu_0 = 4\pi \times 10^{-7}$ H/m, and the dielectric constant ε(F/m) is related to the inhomogeneous refractive-index profile via

$$n^2(x,t) = \mu_0 \varepsilon(x,t). \tag{4}$$

If the rapid oscillatory temporal variation of e_x for optical frequencies is separated out in the form

$$e_x(x,y,z;t) = E_x(x,y,z;t)\exp(i\omega t), \tag{5}$$

Eq. (3) can be written

$$\nabla^2 E_x(x,y,z;t) + \omega^2\mu_0\left[\varepsilon(x,t) - \frac{i\partial\varepsilon(x,t)}{\omega\partial t}\right]E_x(x,y,z;t) = 0. \tag{6}$$

Equation (6) can be further simplified, provided the variation of $\varepsilon(x,t)$ with t is very small for times of the order of ω^{-1}, i.e.,

$$\frac{(\partial\varepsilon/\partial t)_{t\approx\omega^{-1}}}{\varepsilon(t)} \ll 1. \tag{7}$$

Condition (7) is easily met in the case of slowly changing concentration gradients of an electrochemical system so that Eq. (6) becomes

$$\nabla^2 E_x(x,y,z;t) + k_0^2 n^2(x,t) E_x(x,y,z;t) = 0, \tag{8}$$

where $n(x,t)$ is given by Eq. (2) and k_0 is the magnitude of the wave vector for field propagation in a vacuum. The refractive-index profile of Eq. (2) is real and indicates that the propagating beam will suffer neither gain nor loss in the region of the electrolyte. Use of the series expansion for the complementary error function of Eq. (2)[14] and retention of the lowest-order term in $(x/2\sqrt{Dt})$ give the following expression for the refractive-index profile valid for times that are long compared with the chemical species diffusion time τ_d:

$$n(x,t)|_{t>\tau_d} \cong n_0\left[1 - \frac{A}{\sqrt{\pi}}\left(\frac{x}{\sqrt{Dt}}\right) + 0\left(\frac{x}{\sqrt{Dt}}\right)^3\right], \tag{9}$$

where

$$\tau_d \equiv x^2/(4D), \tag{10}$$

$$A \equiv \frac{C_0(\partial n/\partial C)_{C=C_0}}{n_0 + C_0(\partial n/\partial C)_{C=C_0}} \cong \left(\frac{C_0}{n_0}\right)\left(\frac{\partial n}{\partial C}\right)_{C=C_0} \ll 1. \tag{11}$$

Inserting Eq. (9) into Eq. (8) and recognizing the smallness of the constant A, we obtain

$$\nabla^2 E_x + k_0^2 n_0^2\left[1 - \left(\frac{2A}{\sqrt{\pi Dt}}\right)x + \left(\frac{A^2}{\pi Dt}\right)x^2\right]E_x = 0, \tag{12}$$

where only terms up to $0(A^2)$ were retained.

Equation (12) can be solved explicitly for a wave propagating in the z direction, using the substitution

$$E_x(x,y,z;t) = G(x,y,z;t)\exp(-ik_0 n_0 z) \tag{13}$$

and assuming that the longitudinal variation of G is slow enough,[15] so that

$$\frac{\partial^2}{\partial z^2}G(x,y,z;t) \cong 0. \tag{14}$$

Expressing G in the general form[16]

$$G(x,y,z;t) = \exp\{-i[\tfrac{1}{2}Q_x(z,t)x^2 + \tfrac{1}{2}Q_y(z,t)y^2 + S_x(z,t)x + S_y(z,t)y + P(z,t)]\}, \tag{15}$$

substituting Eqs. (13)–(15) into Eq. (12), and equating equal powers of x and y, it can be shown that the parameters Q_x, Q_y, S_x, S_y, and P are governed by the following set of equations[16]:

$$Q_y^2(z,t) + k_0 n_0 \frac{\partial}{\partial z}Q_y(z,t) = 0; \tag{16a}$$

$$Q_x^2(z,t) + k_0 n_0 \frac{\partial}{\partial z}Q_x(z,t) + k_0 n_0 k_{2_x}(t) = 0; \tag{16b}$$

$$Q_y(z,t)S_y(z,t) + k_0 n_0 \frac{\partial}{\partial z}S_y(z,t) = 0; \tag{16c}$$

$$Q_x(z,t)S_x(z,t) + k_0 n_0 \frac{\partial}{\partial z}S_x(z,t) + \tfrac{1}{2}k_0 n_0 k_{1_x}(t) = 0; \tag{16d}$$

$$\frac{\partial}{\partial z}P(z,t) + \frac{i}{2k_0 n_0}[Q_x(z,t) + Q_y(z,t)] + \frac{1}{2k_0 n_0}[S_x^2(z,t) + S_y^2(z,t)] = 0. \tag{16e}$$

In Eqs. (16) the following parameters were defined:

$$k_{1_x}(t) \equiv \frac{2k_0 A}{\sqrt{\pi Dt}}, \tag{17a}$$

$$k_{2_x}(t) \equiv -\frac{k_0 A^2}{\pi Dt}. \tag{17b}$$

In Eqs. (15) and (16) the functions $Q_x(z,t)$ and $Q_y(z,t)$ represent the complex laser beam parameters which govern the size of the beam and the curvature of the phase fronts. The functions $S_x(z,t)$ and $S_y(z,t)$ are the complex displacement parameters which determine the location of the beam. The function $P(z,t)$ is the complex phase parameter which governs the amplitude and phase of the beam. It is also convenient to make the following parameter definitions:

$$k \equiv k_0 n_0; \tag{18a}$$

$$m(t) \equiv \frac{A^2}{\pi Dt} \ll 1. \tag{18b}$$

The set of Eqs. (16) is equivalent to the original wave equation [Eq. (12)]. The solutions are given in terms of well-known measurable laser beam parameters at the beam waist. Equations (16a) and (16b) are of the Riccati type, and their solutions are[17,18]

$$Q_y(z) = \frac{k}{z + q_{0y}}, \tag{19}$$

$$Q_x(z,t) = k\sqrt{m}\left(\frac{\sinh\sqrt{m}z + \zeta\cosh\sqrt{m}z}{\cosh\sqrt{m}z + \zeta\sinh\sqrt{m}z}\right), \tag{20}$$

where

$$q_{0y} \equiv \frac{k}{Q_y(z=0)}, \tag{21}$$

$$\zeta(t) \equiv \frac{Q_x(z=0)}{k\sqrt{m(t)}} = \frac{1}{q_{0x}\sqrt{m(t)}}. \tag{22}$$

Equation (16c) has the solution

$$S_y(z) = S_y(0)\left(\frac{q_{0y}}{z + q_{0y}}\right). \tag{23}$$

To solve Eq. (16d), the transformation

$$S_x(z,t) = S_x'(z,t) - \frac{2}{\sqrt{m}}Q_x(z,t) \tag{24}$$

reduces Eq. (16d) to an equation for $S_x'(z,t)$ which is identical to Eq. (16c).[16] Solving this equation and using Eq. (24) give

$$S_x(z,t) = \frac{S_x(0) + k[\zeta(1 - \cosh\sqrt{m}z) - \sinh\sqrt{m}z]}{\cosh\sqrt{m}z + \zeta\sinh\sqrt{m}z}. \tag{25}$$

Finally, to solve Eq. (16e), the transformation

$$P(z,t) = P'(z,t) - \frac{1}{\sqrt{m}}S_x(z,t) - \frac{1}{2m}Q_x(z,t) - \frac{kz}{2} \tag{26}$$

can be used to obtain the equation

$$\frac{\partial}{\partial z}P'(z,t) + \frac{i}{2k}[Q_x(z,t) + Q_y(z)] + \frac{1}{2k}[(S_x')^2 + S_y^2](z,t) = 0. \tag{27}$$

Solving Eq. (27) and substituting the solution in Eq. (26), along with the solutions for $S_x(z,t)$ and $Q_x(z,t)$, Eqs. (24) and (20), respectively, give the following equation for $P(z,t)$, the complex phase parameter

$$\begin{aligned} P(z,t) = {} & P(0) + \frac{1}{\sqrt{m}}S_x(0) + \frac{k}{2mq_{0x}} \\ & - \frac{i}{2}\left[\ln(\cosh\sqrt{m}z + \zeta\sinh\sqrt{m}z) + \ln\left(1 + \frac{z}{q_{0y}}\right)\right] \\ & - \frac{1}{2k_0}S_y^2(0)\left(\frac{zq_{0y}}{z + q_{0y}}\right) \\ & - \frac{[S_x(0) + k\zeta]^2}{2k\sqrt{m}}\left(\frac{\sinh\sqrt{m}z}{\cosh\sqrt{m}z + \zeta\sinh\sqrt{m}z}\right) \\ & - \frac{1}{\sqrt{m}}\left\{\frac{S_x(0) + k[\zeta(1 - \cosh\sqrt{m}z) - \sinh\sqrt{m}z]}{\cosh\sqrt{m}z + \zeta\sinh\sqrt{m}z}\right\} - \tfrac{1}{2}kz \\ & - \frac{k}{2\sqrt{m}}\left(\frac{\sinh\sqrt{m}z + \zeta\cosh\sqrt{m}z}{\cosh\sqrt{m}z + \zeta\sinh\sqrt{m}z}\right). \end{aligned} \tag{28}$$

IV. Beam Parameter Evolution in Terms of the Solutions of the Beam Equations

Recognizing that the functions Q_x, Q_y, S_x, S_y, and P can be complex, so as to give information about the experimentally measurable laser beam parameters, we can use the following definitions[16]:

$$Q_x(z) = Q_{xr}(z,t) + iQ_{xi}(z,t); \tag{29a}$$

$$Q_y(z) = Q_{yr}(z) + iQ_{yi}(z); \tag{29b}$$

$$S_x(z,t) = S_{xr}(z,t) + iS_{xi}(z,t); \tag{29c}$$

$$S_y(z) = S_{yr}(z) + iS_{yi}(z); \tag{29d}$$

$$P(z,t) = P_r(z,t) + iP_i(z,t). \tag{29e}$$

Complex beam radii q can now be introduced in the x and y coordinates independently:

$$\frac{1}{q_x(z,t)} \equiv \frac{Q_x(z,t)}{k} \equiv \frac{1}{R_x(z,t)} - i\frac{\lambda}{\pi W_x^2(z,t)}, \tag{30a}$$

$$\frac{1}{q_y(z)} \equiv \frac{Q_y(z)}{k} \equiv \frac{1}{R_y(z)} - i\frac{\lambda}{\pi W_y^2(z)}, \tag{30b}$$

where $W_x(z,t)$ and $W_y(z)$ are the spot sizes in the x and y directions, respectively, with the coordinates shown in Fig. 1, and $R_x(z,t)$ and $R_y(z)$ are the radii of curvature of the spherical phase fronts. Using Eqs. (19) and (20) in (30a) and (30b), it can be shown that

$$R_x(z,t) = \frac{\sqrt{m}z_{0x}^2}{1+mz_{0x}^2}\left[\coth\sqrt{m}z + \left(\frac{1}{mz_{0x}^2}\right)\tanh\sqrt{m}z\right], \tag{31a}$$

$$R_y(z) = z\left[1 + \left(\frac{z_{0y}}{z}\right)^2\right]. \tag{31b}$$

Also

$$W_x^2(z,t) = W_{0x}^2\left[\cosh^2\sqrt{m}z + \left(\frac{1}{mz_{0x}^2}\right)\sinh^2\sqrt{m}z\right], \tag{32a}$$

$$W_y^2(z) = W_{0y}^2\left[1 + \left(\frac{z}{z_{0y}}\right)^2\right]. \tag{32b}$$

In Eqs. (31) and (32) W_{0x}, W_{0y} are the spot sizes at the beam waist ($z = 0$), and z_{0x}, z_{0y} are the magnitudes of the complex beam radii, q_{0x} and q_{0y}, assumed to be purely imaginary[15]:

$$q_{0x} \equiv iz_{0x} = i\frac{\pi W_{0x}^2}{\lambda}, \tag{33a}$$

$$q_{0y} \equiv iz_{0y} = i\frac{\pi W_{0y}^2}{\lambda}. \tag{33b}$$

Inserting Eqs. (29a)–(29e) into Eq. (15) and separating the real and imaginary parts yield

$$\begin{aligned} G(x,y,z;t) = \exp(-i\{&\tfrac{1}{2}Q_{xr}(z,t)[x - x_p(z,t)]^2 \\ &+ \tfrac{1}{2}Q_{yr}(z)(y - y_p)^2 - \tfrac{1}{2}Q_{xr}(z,t)x_p^2(z,t) - \tfrac{1}{2}Q_{yr}(z)y_p^2 \\ &+ P_r(z,t)\}) \exp\{\tfrac{1}{2}Q_{xi}(z,t)[x - x_a(z,t)]^2 \\ &+ \tfrac{1}{2}Q_{yi}(z)(y - y_a)^2 \\ &- \tfrac{1}{2}Q_{xi}(z,t)x_a^2(z,t) - \tfrac{1}{2}Q_{yi}(z)x_y^2 + P_i(z,t)\}, \end{aligned} \tag{34}$$

where[16]

$$x_p(z,t) \equiv -\frac{S_{xr}(z,t)}{Q_{xr}(z,t)}, \tag{35a}$$

$$x_a(z,t) \equiv -\frac{S_{xi}(z,t)}{Q_{xi}(z,t)}, \tag{35b}$$

with similar definitions for y_p and y_a. In Eqs. (35), $x_p(y_p)$ is the displacement in the $x - (y-)$ direction of the phase-front center, while $x_a(y_a)$ is the displacement in the $x - (y-)$ direction of the center of the amplitude distribution. Inserting the definitions, Eqs. (33) in Eqs. (19), (20), (23), (25), and (28), the following expressions are obtained for the real and imaginary parts of the beam parameters Q_x, Q_y, S_x, S_y, and P:

$$Q_{xr}(z,t) = \frac{k}{R_x(z,t)}; \tag{36}$$

$$Q_{xi}(z,t) = -\frac{2}{W_x^2(z,t)}; \tag{37}$$

$$Q_{yr}(z) = \frac{k}{R_y(z)}; \tag{38}$$

$$Q_{yi}(z) = -\frac{2}{W_y^2(z)}; \tag{39}$$

$$S_{xr}(z,t) = k\left\{\frac{[s_{0x} + g(1 - \cosh\sqrt{m}z)]g - \cosh\sqrt{m}z}{\sqrt{m}(1+g^2)R_x(z,t)\cosh\sqrt{m}z}\right\}, \tag{40}$$

where s_{0x} and g are defined by

$$S_x(0) \equiv -iks_{0x}, \tag{41}$$

$$g \equiv i\zeta = 1/\sqrt{m}z_{0x}. \tag{42}$$

Also

$$S_{xi}(z,t) = -k\left[\frac{W_{0x}}{W_x(z,t)}\right]^2[(s_{0x} + g)\cosh\sqrt{m}z - g], \tag{43}$$

$$S_{yr}(z) = k\frac{s_{0y}z_{0y}}{R_y(z)}, \tag{44}$$

where s_{0y} is defined by

$$S_y(0) \equiv -iks_{0y}. \tag{45}$$

Similarly,

$$S_{yi}(z) = -\frac{s_{0y}z_{0y}}{W_y^2(z)}. \tag{46}$$

Finally,

$$\begin{aligned} P_r(z,t) = P_r(0) &- \tfrac{1}{2}[\eta_x(z,t) + \eta_y(z)] + k\frac{(s_{0y}z_{0y})^2}{2R_y(z)} - \frac{kz}{2} \\ &+ k\left[\frac{s_{0x}^2 + 2g^2 + 1 + 2g(s_{0x} + g)(\cosh\sqrt{m}z - 1)}{2m(1+g^2)R_x(z,t)\cosh\sqrt{m}z}\right], \end{aligned} \tag{47}$$

$$\begin{aligned} P_i(z,t) = P_i(0) &- \tfrac{1}{4}\left\{\ln(\cosh^2\sqrt{m}z + g^2\sinh^2\sqrt{m}z) + \ln\left[1 + \left(\frac{z}{z_{0y}}\right)^2\right]\right\} \\ &+ \frac{(s_{0y}z)^2}{W_y^2(z)} + \frac{(z_{0x}/\sqrt{m})}{W_x^2(z,t)}[(s_{0x}^2 + 1)g\sinh^2\sqrt{m}z + 2(s_{0x} + g) \\ &\times (1 - \cosh\sqrt{m}z)\cosh\sqrt{m}z], \end{aligned} \tag{48}$$

where

$$\eta_x(z,t) \equiv \tan^{-1}(g\tanh\sqrt{m}z), \tag{49a}$$

$$\eta_y(z) \equiv \tan^{-1}(z/z_{0y}). \tag{49b}$$

Equations (29)–(49) are explicit functional forms describing the evolution of the various laser beam parameters: In the x direction $Q_{xr}(z,t)$, Eq. (30a), is a measure of the radius of curvature $R_x(z,t)$ of the spherical phase fronts in the x-z plane. $Q_{xi}(z,t)$, Eq. (30a), is a measure of the evolution of the $1/e$ spot size $W_x(z,t)$ along the x axis. $S_{xr}(z,t)$, Eq. (40), shows the

evolution of the displacement of the phase-front center in the x direction, and $S_{xi}(z,t)$, Eq. (43), is a measure of the beam centroid displacement. The function $P_r(z,t)$, Eq. (47), describes the evolution of the phase of the beam in the direction of propagation, and the function $P_i(z,t)$, Eq. (48), gives the amplitude distribution along the x axis for any position $z \geq 0$ at time t.

Similar interpretations in the y direction can be given to the quantities $Q_{yr}, Q_{yi}, S_{yr}, S_{yi}$.

V. Beam Equations in the Limit $m(t) \ll 1$

The time dependence of the beam parameters enters the beam equations only through the quantity $m(t)$, Eq. (18b). In view of the smallness of this parameter in practical electrochemical systems, the beam equations which were obtained in Sec. IV for a general $m(t)$ can be simplified considerably upon expanding the hyperbolic functions sinh and cosh according to

$$\cosh x \cong 1 + \frac{x^2}{2}; \quad x \ll 1, \tag{50a}$$

$$\sinh x \cong x; \quad x \ll 1, \tag{50b}$$

and retaining terms of $0[m(t)]$ and lower. Only the x-coordinate dependent parameters are affected by this simplification:
from Eq. (31a)

$$R_x(z,t) \cong z\left[\frac{(1+mz_{0x}^2)+(z_{0x}/z)^2}{1+m(z_{0x}^2+\tfrac{1}{2}z^2)}\right]; \tag{51}$$

from Eq. (32a)

$$W_x^2(z,t) \cong W_{0x}^2[(1+mz^2)+(z/z_{0x})^2]; \tag{52}$$

from Eq. (40)

$$S_{xr}(z,t) \cong \frac{k}{R_x(z,t)}\left[\frac{s_{0x}z_{0x}-\sqrt{m}\left(z_{0x}^2+\frac{z^2}{2}\right)}{1+m\left(z_{0x}^2+\frac{z^2}{2}\right)}\right]; \tag{53}$$

from Eq. (43)

$$S_{xi}(z,t) \cong -k\left[\frac{W_{0x}}{W_x(z,t)}\right]^2\left[s_{0x}\left(1+\frac{mz^2}{2}\right)+\frac{\sqrt{m}}{2}\frac{z^2}{z_{0x}}\right]; \tag{54}$$

from Eq. (47)

$$\begin{aligned} P_r(z,t) \cong P_r(0) &- \tfrac{1}{2}\left\{\tan^{-1}\left[\frac{(z/z_{0x})}{1+m(z^2/2)}\right]+\tan^{-1}(z/z_{0y})\right\} \\ &+ k\frac{(s_{0y}z_{0y})^2}{2R_y(z)} - \frac{kz}{2} + \frac{k}{2R_x(z,t)}\{[z_{0x}^2(1+s_{0x}^2)+z^2 \\ &+ \sqrt{m}s_{0x}z_{0x}z^2 + (mz_{0x}^2z/2)(1+s_{0x}^2)]/ \\ &[1+m(z_{0x}^2+z^2/2)]\}; \end{aligned} \tag{55}$$

and from Eq. (48)

$$\begin{aligned} P_i(z,t) = P_i(0) &- \tfrac{1}{4}\ln\{[(1+mz^2)+(z/z_{0x})^2][1+(z/z_{0y})^2]\} \\ &+ \frac{(s_{0y}z)^2}{W_y^2(z,t)} + \frac{z^2(s_{0x}^2-\sqrt{m}s_{0x}z_{0x}-mz^2/2)}{W_x^2(z,t)}. \end{aligned} \tag{55'}$$

Insertion of Eqs. (36), (37), (40), and (43) in Eqs. (35a) and (35b) gives for the displacement parameters

$$x_a(z,t) = m^{-1/2} - (s_{0x}z_{0x}+m^{-1/2})\cosh\sqrt{m}z, \tag{56a}$$

$$x_p(z,t) = m^{-1/2}\left[\frac{(1+mz_{0x}^2)\cosh\sqrt{m}z - 1 - \sqrt{m}s_{0x}z_{0x}}{(1+mz_{0x}^2)\cosh\sqrt{m}z}\right]. \tag{56b}$$

In the limit of $m \ll 1$, Eqs. (56a) and (56b) become

$$x_a(z,t) \cong -s_{0x}z_{0x}(1+mz^2/2) - \sqrt{m}z^2/2, \tag{57a}$$

$$x_p(z,t) \cong \frac{-s_{0x}z_{0z}+\sqrt{m}\left(z_{0x}^2+\frac{z^2}{2}\right)}{1+m\left(z_{0x}^2+\frac{z^2}{2}\right)}. \tag{57b}$$

The amplitude and phase of the electromagnetic field can now be computed explicitly from Eqs. (13) and (34), using the parameter functions in the limit $m(t) \ll 1$:

A. Amplitude of the Electric Field Vector

$$\begin{aligned} |E_x(x,y,z;t)| = E_0\left[\frac{W_{0x}W_{0y}}{W_x(z,t)W_y(z)}\right]^{1/2} &\exp\left[\frac{y_a^2+s_{0y}^2z^2}{W_y^2(z)}\right. \\ &\left.+\frac{x_a^2+z^2(s_{0x}^2-\sqrt{m}s_{0x}z_{0x}-mz^2/2)}{W_x^2(z,t)}+P_i(0)\right] \\ &\times\exp\left[-\frac{(x-x_a)^2}{W_x^2(z,t)}-\frac{(y-y_a)^2}{W_y^2(z,t)}\right]. \end{aligned} \tag{58}$$

Imposing the boundary conditions on the amplitude distribution centroids,

$$x_a(0,t) = x_0, \tag{59a}$$

$$y_a(0,t) = y_0, \tag{59b}$$

the (so far arbitrary) constants s_{0x}, s_{0y} take the values

$$s_{0x} = -x_0/z_{0x} \qquad s_{0y} = -y_0/z_{0y},$$

and the equations for the beam intensity centroid can be written

$$x_a(z,t) = x_0\left(1+\frac{mz^2}{2}\right) - \frac{\sqrt{m}}{2}z^2, \tag{60a}$$

$$y_a(z) = y_0, \tag{60b}$$

$$x_p(z,t) = \frac{x_0+\sqrt{m}(z_{0x}^2+z^2/2)}{1+m(z_{0x}^2+z^2/2)}, \tag{60c}$$

$$y_p(z) = y_0. \tag{60d}$$

Inserting Eqs. (60) in (58) and setting the (so far arbitrary) constant $P_i(0)$ equal to

$$-\left(\frac{x_0^2}{W_{0x}^2}+\frac{y_0^2}{W_{0y}^2}\right),$$

the amplitude of the electric field vector of the propagating laser beam is given by

$$\begin{aligned} |E_x(x,y,z;t)| = E_0\left[\frac{W_{0x}W_{0y}}{W_x(z,t)W_y(z)}\right]^{1/2} \\ \times\exp\left\{-\frac{[x-x_a(z,t)]^2}{W_x^2(z,t)}-\frac{(y-y_0)^2}{W_y^2(z)}\right\}, \end{aligned} \tag{61}$$

where the various quantities are given by Eqs. (32a), (32b), and (56a) or, in their $m(t) \ll 1$ limits, by Eqs. (52) and (60a).

B. Phase of the Electric Field Vector

On writing $E_x(x,y,z;t) = |E_x(x,y,z;t)| \exp[-i\phi(x,y,z;t)]$, the phase of the electric field vector of

the laser beam propagating in the fluid electrolyte can be identified from Eqs. (13) and (34) as follows:

$$\phi(x,y,z;t) = \tfrac{1}{2}Q_{xr}(z,t)(x-x_p)^2 + \tfrac{1}{2}Q_{yr}(z)(y-y_p)^2 - \tfrac{1}{2}Q_{xr}(z,t)x_p^2 - \tfrac{1}{2}Q_{yr}(z)y_p^2 + P_r(z,t) + kz. \quad (62)$$

Inserting Eqs. (36), (38), (60c), (60d), and (55) in Eq. (62) and setting the orbitrary constant $P_r(0) = 0$, it can be shown that

$$\phi(x,y,z;t) = \frac{k}{2}\left\{\frac{[x-x_p(z,t)]^2}{R_x(z,t)} + \frac{(y-y_0)^2}{R_y(z)} + \frac{z^2}{R_x(z,t)}\left\{\frac{(1-\sqrt{m}x_0)^2[1+(z_{0x}/z)^2]}{1+2m(z_{0x}^2+z^2/2)}\right\}\right\} + \tfrac{1}{2}\left\{kz - \tan^{-1}\left[\frac{(z/z_{0x})}{[1+m(z^2/2)]}\right] - \tan^{-1}(z/z_{0y})\right\}. \quad (63)$$

Finally, the laser beam intensity is given by[19]

$$I(x,y,z;t) = \frac{1}{2\eta}\,\mathbf{E}_x \cdot \mathbf{E}_x^* \ (\mathrm{W/m^2}), \quad (64)$$

where $\eta(\Omega)$ is the wave impedance of the fluid electrolyte medium. Equation (64) can be written in terms of the incident beam intensity I_0 at $z = 0$:

$$I(x,y,z;t) = I_0\left[\frac{W_{0x}W_{0y}}{W_x(z,t)W_y(z)}\right] \times \exp\left\{-2\left\{\frac{[x-x_a(z,t)]^2}{W_x^2(z,t)} + \frac{(y-y_0)^2}{W_y^2(z)}\right\}\right\}. \quad (65)$$

VI. Ray-Optic Limit

(1) The laser beam intensity field obtained in Sec. V is consistent in the limit of Eq. (9), i.e., for $x^2 < 4Dt$, with a simpler treatment of the beam in the ray-optic approximation. In that approximation, no information about the spatial or temporal intensity distribution can be obtained. However, the equation of motion of the beam intensity centroid $x_a(z,t)$ can be correctly described by ray optics. Equations (16b) and (16d) and the definition (35b) of x_a yield

$$\frac{\partial^2}{\partial z^2}x_a(z,t) + \left[\frac{k_{2x}(t)}{k}\right]x_a(z,t) + \tfrac{1}{2}\left[\frac{k_{1x}(t)}{k}\right] = 0. \quad (66)$$

Equation (66) can be written in terms of the components of the refractive index:

$$n(x,t) \cong n_0\left\{1 - \left(\frac{n_{1x}}{2n_0}\right)x - \left(\frac{n_{2x}}{2n_0}\right)x^2\right\}, \quad (67)$$

where

$$n_{1x}(t) = k_{1x}(t)/k_0, \quad (68a)$$

$$n_{2x}(t) = k_{2x}(t)/k_0. \quad (68b)$$

Equations (66)–(68) result in the following equation for x_a:

$$n_0\frac{\partial^2}{\partial z^2}x_a(z,t) = -\tfrac{1}{2}n_{1x}(t) - n_{2x}(t)x_a(z,t) \quad (69)$$

or

$$n_0\frac{\partial^2}{\partial z^2}x_a(z,t) = -\frac{\partial}{\partial x}n(x,t)|_{x=x_a(z,t)}, \quad (69')$$

which is the paraxial ray equation of ray optics for a refractive-index field $n(x,t)$ which decreases with increasing x.

Using Eqs. (17a) and (17b) in (67) and solving Eq. (69′) we find the beam displacement in the ray-optic approximation:

$$x_a(z,t) = m^{-1/2} + [x_a(0,t) - m^{-1/2}]\cosh\sqrt{m}z + m^{-1/2}\left(\left.\frac{\partial x_a}{\partial z}\right|_{z=0}\right)\sinh\sqrt{m}z. \quad (70)$$

The boundary conditions

$$x_a(0,t) = x_0, \text{ for the initial displacement,}$$

$$\left.\frac{\partial x_a}{\partial z}\right|_{z=0} \equiv x_0' = 0, \text{ for the initial beam deflection,}$$

along with $m(t) \ll 1$, simplify Eq. (70):

$$x_a(z,t) = x_0\left(1 + \frac{mz^2}{2}\right) - \frac{\sqrt{m}}{2}z^2,$$

which is identical to Eq. (60a) which was obtained using a wave-optics model. The beam deflection can be obtained from $x_a(z,t)$ upon differentiating

$$\theta(x,t) = \frac{\partial}{\partial z}x_a(z,t) = -(1-\sqrt{m}x_0)\sinh\sqrt{m}z + x_0'\cosh\sqrt{m}z. \quad (71)$$

Equation (71) can be simplified for the special case considered here to give

$$\theta(z,t) \cong -\left(\frac{A}{\sqrt{\pi Dt}} - \frac{A^2x_0}{\pi Dt}\right)z. \quad (72)$$

In the geometry of Fig. 1, $\theta(z,t) < 0$ indicates that for an incident laser beam which is initially parallel to the electrode plane, the subsequent deflection will be toward the surface of the electrode, i.e., in the direction of the refractive-index gradient $\nabla_c n$. In the wave-optics picture, Eq. (72) indicates the deflection of the beam intensity centroid.

(2) General expressions for the beam centroid displacement $x_a(z,t)$ and beam deflection $\theta(z,t)$, valid for all experimentally useful times, can be obtained from a ray-optic model using a perturbational method of solution of the nonlinear paraxial ray equation, provided that $A \ll 1$ [Eq. (11)]. The refractive-index profile of Eq. (2), when inserted in the paraxial ray equation (69′), yields the following nonlinear equation for the beam centroid displacement:

$$\frac{d^2x_a(z,t)}{dz^2} + \frac{A}{\sqrt{\pi Dt}}\exp\left[-\frac{x_a^2(z,t)}{4Dt}\right] = 0. \quad (73)$$

For time-domain studies of conventional electrochemical systems $t \gtrsim 0.1$ sec,[20,21] so that $(A/\sqrt{\pi Dt}) = \sqrt{m(t)} \equiv \delta < 1$. x_a can be expanded in terms of a power series in δ:

$$x_a(z,t) = \sum_{k=0}^{\infty}\delta^k X_k(z,t) \quad (74)$$

subject to the boundary conditions

$$X_0(0,t) = x_0, \quad (75a)$$

$$X_j(0,t) = 0; \qquad j \neq 0, \quad (75b)$$

$$\frac{d}{dz}X_k(z,t)|_{z=0} = 0; \qquad k = 0,1,2,\ldots. \tag{75c}$$

Insertion of Eq. (74) in (73) and retention of terms of order δ^2 or less give the following coupled equations for the first three terms X_0, X_1, and X_2:

$$\frac{d^2}{dz^2}X_0(z,t) = 0; \tag{76a}$$

$$\frac{d^2}{dz^2}X_1(z,t) + \exp\left[-\frac{X_0^2(z,t)}{4Dt}\right] = 0; \tag{76b}$$

$$\frac{d^2}{dz^2}X_2(z,t) - \frac{X_0(z,t)X_1(z,t)}{2Dt}\exp\left[-\frac{X_0^2(z,t)}{4Dt}\right] = 0. \tag{76c}$$

Solution of Eqs. (76) subject to Eqs. (75) and use of Eq. (74) give

$$x_a(z,t) = x_0 - \frac{\sqrt{m}z^2}{2}\left(1 + \frac{\sqrt{m}x_0z^2}{24Dt}\right)\exp\left(-\frac{x_0^2}{4Dt}\right) \tag{77}$$

accurate to order δ^2. The beam deflection can now be calculated:

$$\theta(z,t) = -\sqrt{m}z\left[1 + \frac{\sqrt{m}x_0z^2}{12Dt}\right]\exp\left(-\frac{x_0^2}{4Dt}\right). \tag{78}$$

Equations (77) and (78) can be seen to reduce to Eqs. (60a) and (72) in the special case $x_0^2 < 4Dt$.

VII. Discussion—Results

Figures 2 and 3 show numerical results for the beam intensity centroid displacement, Eq. (77), and beam deflection, Eq. (78), respectively. The advantage of the mathematical perturbation method used for those calculations is the ability to study quantitatively laser beam dynamics at all times of interest in an electrochemical experiment. Figure 2 shows the expected departure of the beam centroid toward the electrode surface, i.e., toward the region of increased refractive index, at early times. As the refractive-index gradient, $[\partial/(\partial x)]n(x,t)$, decreases for times $t \gg x_0^2/(4D)$, the concentration of the chemical species under consideration becomes essentially uniform throughout the electrolyte, $C(x,t) \to C_0$ in Eq. (1). At the limit $t = \infty$, the electrolyte acquires a uniform refractive index:

$$n(x,\infty) = n_0 + C_0\left(\frac{\partial n}{\partial C}\right)_{C=C_0} \cong n_0$$

in Eq. (2). Therefore, any departure of the beam intensity centroid toward the electrode tends to be negligible, as shown in Fig. 2. Similar features to those of Fig. 2 can be seen in the behavior of the beam deflection in Fig. 3. In both figures, the position of the beam detector was assumed to be at $z = z^* = 3$ cm. The minima of the curves shown in Figs. 2 and 3 correspond to diffusion times,

$$\tau_{d_0} = x_0^2/4D,$$

and they shift to later times for larger beam axis offset values x_0. Due to the 1-D inhomogeneity in the refractive-index profile along only the x axis of Fig. 1, no beam deflection occurs along the y axis in the present model.

Preliminary experimental observations have indicated an asymmetric spot shape with respect to the beam centroid at early times, before the minima at $t = \tau_{d_0}$ are reached. The experimental spot shape tends to occupy a larger spatial extent along the x axis toward the direction of the electrode surface than away from it. This early time behavior can be qualitatively understood within the framework of the present theory as follows: For times $t \ll \tau_{d_0}$ the refractive-index gradient along the x axis is given from Eq. (2):

$$\frac{\partial}{\partial x}n(x,t) = -(A/\sqrt{\pi Dt})\exp\left(-\frac{x^2}{4Dt}\right),$$

which shows that the gradient is very steep close to the electrode surface, decreasing very rapidly with distance into the electrolyte. The higher value of $\partial n/\partial x$ closer to the surface would tend to enhance the mirage effect in that region. This is expected to result in a more pronounced bending of the part of the beam below the intensity centroid (i.e., closer to the surface) than that

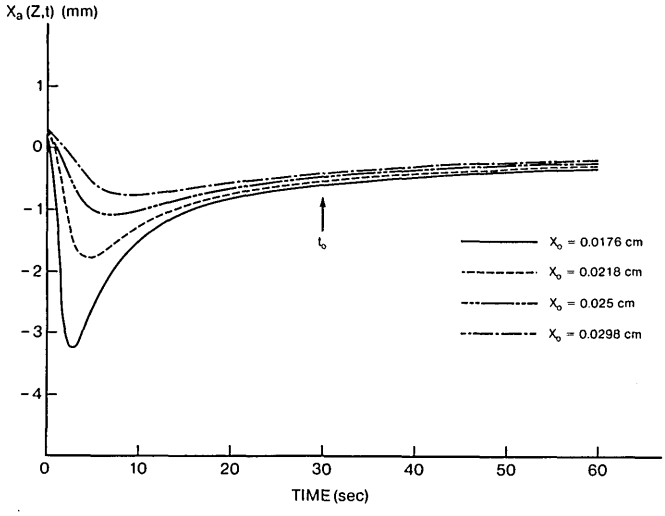

Fig. 2. Beam intensity centroid displacement according to perturbation theoretical expression, Eq. (77). $A = 5.9 \times 10^{-4}$; $D = 1.49 \times 10^{-5}$ cm^2/sec; $z = 3.0$ cm. t_0 corresponds to the intensity profile of Fig. 6.

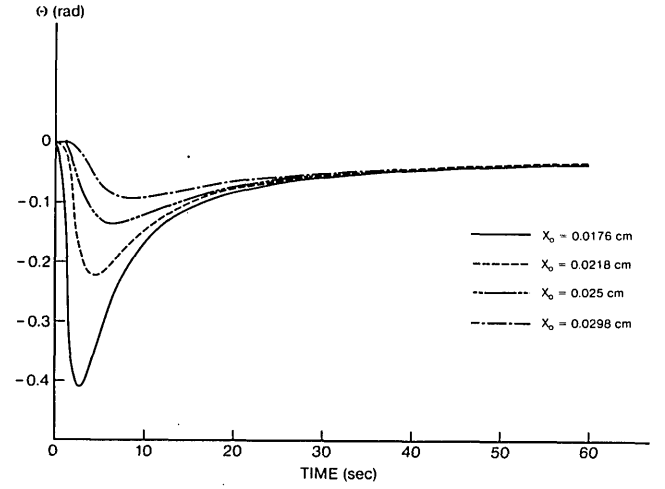

Fig. 3. Beam deflection according to perturbation theoretical expression, Eq. (78). $A = 5.9 \times 10^{-4}$; $D = 1.49 \times 10^{-5}$ cm^2/sec; $z = 3.0$ cm.

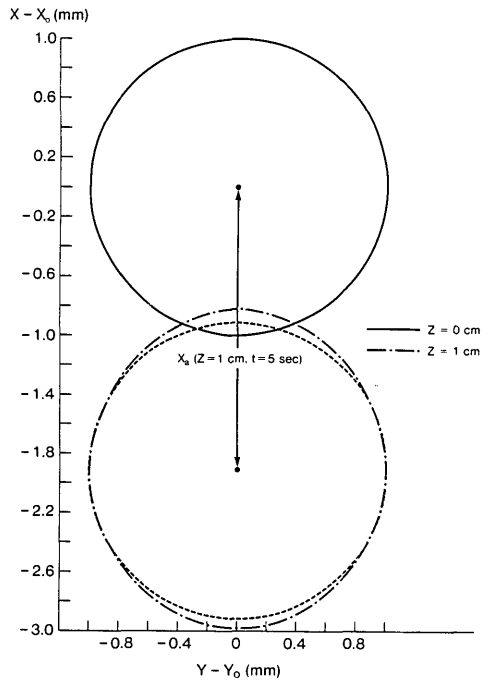

Fig. 4. Fundamental mode He–Ne laser beam spot shapes, Eq. (79), and beam centroid displacement for two positions of the intensity profile detector. $x_0 = y_0 = 0.0176$ cm; $D = 1.49 \times 10^{-5}$ cm^2/sec; $A = 5.9 \times 10^{-3}$; $t = 5$ sec. The dashed line circle in the lower spot shape has been drawn to emphasize its elliptic character.

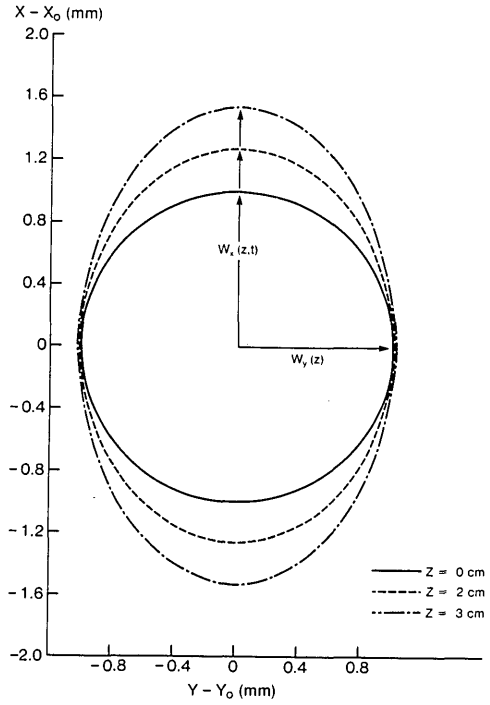

Fig. 5. Fundamental mode He–Ne laser beam spot shapes, Eq. (79), for three positions of the intensity profile detector. All spot shapes were drawn concentrically to emphasize the spatial development of the ellipse. $x_0 = y_0 = 0.0176$ cm; $D = 1.49 \times 10^{-5}$ cm^2/sec; $A = 5.9 \times 10^{-3}$; $t = 5$ sec.

above the centroid (i.e., away from the surface), in agreement with our preliminary experimental observations. For times $t \gg \tau_{d0}$, the approximation

$$\exp\left(-\frac{x_0^2}{4Dt}\right) \cong 1$$

is valid. This results in an essentially spatially constant refractive-index gradient,

$$\frac{\partial n}{\partial x} \cong -(A/\sqrt{\pi Dt}),$$

throughout the body of the electrolyte. In this limit, all parts of the laser beam are expected to bend by the same amount, and the intensity profile will be symmetric about the centroid. The wave-optic theory presented in Secs. III and IV is strictly valid for times $t > \tau_d$ in Eq. (10). Under this condition, the solution to Maxwell's equations, Eq. (65), shows that the spot shape of the laser beam emerging from the electrode–electrolyte region is an elliptic Gaussian with time-dependent major axis length. The greatest effect of the inhomogeneous refractive-index profile on the spot shape is expected to occur at relatively early times so that the factor $(mz^2/2)$ within the parentheses in Eq. (60a) will be comparable to unity. Figure 4 shows the spot shape defined by the intensity boundaries corresponding to $1/e^2$ of the incident light intensity, i.e., by the ellipse

$$\frac{[x - x_a(z^*,t)]^2}{W_x^2(z^*,t)} + \frac{(y - y_0)^2}{W_y^2(z^*)} = 1 \tag{79}$$

with the beam waist centered at (x_0,y_0).

At the entrance to the electrode–electrolyte system (detector position $z^* = 0$) was placed the beam waist. Therefore, the spot shape remains circular Gaussian at all times as shown by the upper curve of Fig. 4. At a point $z^* = 1$ cm the beam intensity profile has shifted to a position centered ~1.9 mm below that at the beam waist in the direction of the electrode surface. The spot shape exhibits a slight elliptic character with an increased major axis along the x direction. This is shown by the lower curve of Fig. 4. A concentric circle has also been drawn to emphasize the extent of the elliptic character of the spot shape at $t = 5$ sec.

Figure 5 shows development of the Gaussian ellipse at different beam detector positions z^* with cocentered spot shapes to facilitate the comparison. The elliptic character is seen to be a sensitive function of the detector position at early times ($t = 5$ sec). The length of the major axis W_x contains electrochemical information about the electrode–electrolyte system: For an instant $t = t_0$, a plot of the $W_x^2(z,t_0)$ vs z^2 will give a straight line, whose slope is, according to Eq. (52),

$$\frac{dW_x^2(z,t_0)}{d(z^2)} = W_{0x}^2\left(\frac{A^2}{\pi Dt_0} + \frac{1}{z_{0x}^2}\right). \tag{80}$$

Similarly, for a fixed detector position z^*, a plot of $W_x^2(z^*,t)$ vs t^{-1} will give a straight line with slope:

$$\frac{dW_x^2(z^*,t)}{d(1/t)} = \frac{(z^*)^2 W_{0x}^2 A^2}{\pi D}. \tag{81}$$

For a given laser wavelength and spot size at the beam waist, Eqs. (80) and (81) in conjunction with Fig. 5 can

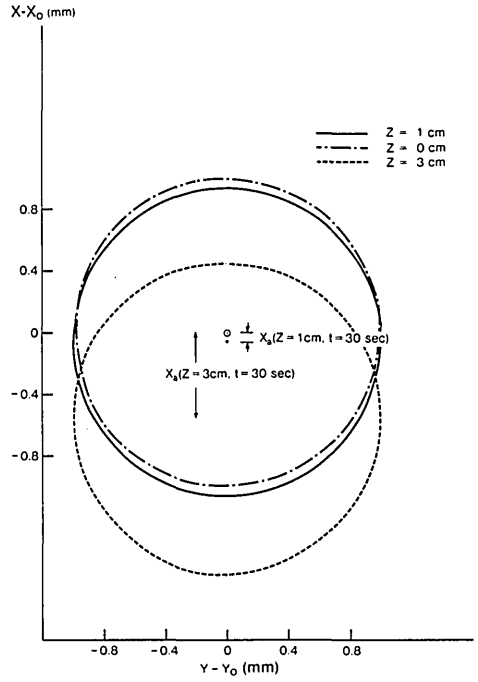

Fig. 6. Fundamental mode He–Ne laser beam spot shapes, Eq. (79), and beam centroid displacements for three positions of the intensity profile detector. $x_0 = y_0 = 0.0176$ cm; $D = 1.49 \times 10^{-5}$ cm^2/sec; $A = 5.9 \times 10^{-4}$; $t = 30$ sec (see Fig. 2).

give quantitative information about the refractive-index gradient $\nabla_c n$ via Eq. (11) and the chemical species diffusion coefficient D, if both plots can be constructed (i.e., W_x^2 vs z^2 and vs t^{-1}).

Figure 6 is a sequence of spot shapes for different beam detector positions at times very long compared to τ_d. For such times concentration and refractive-index gradients are small. Figure 6 shows that the effects of the $\nabla_c n$ on the spot shape at the instant $t_0 = 30$ sec are negligible. That instant corresponds to the time t_0 of Fig. 2. The intensity centroid position is, however, a more sensitive function of $\nabla_c n$ than the spot shape, as shown in Figs. 4 and 6. To first order in A, a plot of x_a vs z^2 at some instant t_0 should give a straight line according to Eq. (60a) with a slope

$$\frac{dx_a(z,t_0)}{d(z^2)} = -\frac{A}{2\sqrt{\pi D t}}, \tag{82}$$

and a plot of x_a vs $t^{-1/2}$ for a fixed detector position z^* should give a straight line with a slope

$$\frac{dx_a(z^*,t)}{d(1/\sqrt{t})} = -A/2\sqrt{\pi D}. \tag{83}$$

Equations (81) and (83) constitute a simple system of two equations with two unknown parameters, A and D, which can be uniquely solved from spot shape and intensity centroid position data in the experimentally convenient configuration using a fixed beam position detector (e.g., a United Detector Technology model UDT SC/25)[5] and a fixed intensity profile detector (e.g., a self-scanning Reticon RA-32x32A photodiode array).[22]

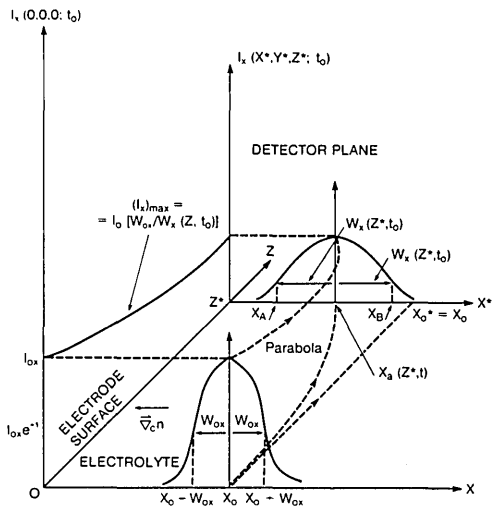

Fig. 7. Qualitative illustration of the intensity spatial profile and displacement of a fundamental Gaussian mode propagation in an optically inhomogeneous electrolyte fluid.

The intensity profile of Eq. (65) exhibits a pre-exponential factor which is time-dependent and increases slightly with increasing t. A numerical evaluation of $[W_{0x} W_{0y}/W_x(z,t) W_y(z)]$ as a function of t for the system parameters of Fig. 6 has shown that the change in intensity due to the pre-exponential factor is <0.1% for $30 \text{ sec} \lesssim t \lesssim 400$ sec.

Figure 7 is a qualitative illustrative plot of the beam intensity profile in the direction of the inhomogeneous refractive-index gradient as a function of propagation distance within the electrolyte. The beam waist is located at $z = 0$, and the position and intensity detectors are located at $z = z^*$. The trajectory of the intensity centroid is assumed parabolic, given for $t_0 > \tau_{d_0}$ by Eq. (60a), and corresponds to the time regime past the minimum of Fig. 2.

The theory presented in this work demonstrates the importance of transverse photothermal deflection spectroscopy for the study of electrochemical processes, such as electrode reaction kinetics, and for the measurement of electrochemical and photoelectrochemical parameters, such as D, A, and $\nabla_c n$. Rossi *et al.*[20] have used diffractive spectroelectrochemistry to study spatial distribution profiles of electrogenerated chromophores at a thin electrode–electrolyte interface. The intensity distribution of a 5-mW He–Ne laser beam diffracted off the platinum electrode adge was recorded in the Fraunhofer region using a photomultiplier tube and was further numerically Fourier transformed to give spatial information about the beam intensity profile at the electrode. Thus these authors were able to construct numerical absorbance vs time profiles corresponding to particular diffraction angles on the photomultiplier aperture plane (screen). A constant refractive index for the electrolyte fluid medium was assumed for the theoretical analysis, and little or no effect of possible spatial variations of the refractive index in their experimental system was claimed. Nevertheless, the experimental data at small angles on the screen showed appreciable deviation from the numerical results of the

model. This was attributed largely to poor accuracy in angle determination and optical alignment. The results of the present theory, however, show the possibility of an elliptic Gaussian beam propagation through the electrolyte regions of highest electrogenerated chromophore concentration due to the presence of a refractive-index gradient. Rossi *et al.* assumed a circular Gaussian beam for their system. The major axis of an elliptical intensity profile, extending farther out from the beam centroid than the radius of the circular profile at the beam waist, Fig. 5, should be expected to contribute more to smaller angles of its Fourier transform on the screen because of the inverse relationship between the spatial Fourier components of the intensities at the electrode and the photomultiplier planes. It is, therefore, possible that a numerical Fourier transform of an elliptic Gaussian intensity profile would weight the small angle, low frequency Fourier components more heavily than the theory by Rossi *et al.* and could diminish, or even account for, the discrepancy among numerical, theoretical, and experimental results at small angles. This discrepancy appears most pronounced at early observation times (<1.0 sec), at which a propagating Gaussian mode is most likely to exhibit strong elliptic character according to results of this work (Figs. 4–6).

VIII. Conclusions

In this work a general wave-optic formalism was developed for treating the propagation of a Gaussian laser beam in an optically inhomogeneous fluid electrolyte with a refractive-index gradient due to a chemical species diffusion from the electrode–electrolyte interface. The theory was shown to be rigorously applicable for times that are long compared with the electrochemical species diffusion time. A ray-optic theory was also developed using a mathematical perturbation technique to describe the beam intensity centroid and deflection at all times of experimental interest. The wave-optic theoretical predictions of the spot shape are consistent with a new interpretation of observed discrepancies between experimental and theoretical diffractive spectroelectrochemical data reported by Rossi *et al.*[20]

The authors would like to thank Jim Dodgson for his helpful assistance with the numerical evaluation of the computer programs. One of us (A.M.) wishes to acknowledge the financial support of the National Science and Engineering Council of Canada which made this research possible. The other author (B.S.H.R.) wishes to acknowledge the support of the National Science Foundation throughout the duration of this work.

References

1. A. J. Bard and L. R. Faulkner, *Electrochemical Methods* (Wiley, New York, 1980).
2. J. O'M. Bockris and S. U. M. Kahn, *Quantum Electrochemistry* (Plenum, New York, 1979).
3. S. R. Morrison, *Electrochemistry at Semiconductor and Oxidized Metal Electrodes* (Plenum, New York, 1980).
4. B. S. H. Royce, S. Sanchez-Sinencio, R. Goldstein, R. Muratore, R. Williams, and W. M. Yim, "Studies of Photocorrosion at the ZnSe-Electrolyte Interface by Photothermal Deflection Spectroscopy," J. Electrochem. Soc. **129,** 2393 (1982).
5. J. G. Mendoza-Alvarez, B. S. H. Royce, F. Sanchez-Sinencio, O. Zelaya-Angel, C. Menzes, and R. Triboulet, "Optical Properties of CdTe Thin Films Studied by Photothermal Deflection Spectroscopy," Thin Solid Films **102,** 259 (1983).
6. J. P. Roger, D. Fournier, and A. C. Boccara, at Third International Conference on Photoacoustic and Photothermal Spectroscopy, Paris, Apr. 1983.
7. A. C. Boccara, D. Fournier, and J. Badoz, "Thermo-Optical Spectroscopy: Detection by the Mirage Effect," Appl. Phys. Lett. **36,** 130 (1980).
8. J. C. Murphy and L. C. Aamodt, "Photothermal Spectroscopy Using Optical Beam Probing: Mirage Effect," J. Appl. Phys. **51,** 4580 (1980); J. Appl. Phys. **52,** 4903 (1981).
9. A. Mandelis, "Absolute Optical Absorption Coefficient Measurements Using Transverse Photothermal Deflection Spectroscopy," J. Appl. Phys. **54,** 3404 (1983).
10. J. Crank *The Mathematics of Diffusion* (Oxford U.P., London, 1975), Chap. 2.
11. W. A. Roth and K. Scheel, Eds., *Landolt-Boernstein, Physikatisch-Chemische Tabellen, Vol. 2* (Springer, Berlin, 1923), Tables 174, 179, 185, 186.
12. R. H. Muller, *Advances in Electrochemistry and Electrochemical Engineering, Vol. 9* (Wiley, New York, 1973), pp. 281–368.
13. E. A. J. Marcatili, "Modes in a Sequence of Thick Astigmatic Lens-Like Focusers," Bell Syst. Tech. J. **44,** 2887 (1964).
14. H. S. Carslaw and J. C. Jaeger, *Conduction of Heat in Solids* (Oxford U.P., London, 1959), Appendix II.
15. A. Yariv, *Quantum Electronics* (Wiley, New York, 1975), Chap. 6.5.
16. L. W. Casperson, "Gaussian Light Beams in Inhomogeneous Media," Appl. Opt. **12,** 2434 (1973).
17. D. L. Kreider, R. G. Kuller, and D. R. Ostberg, *Elementary Differential Equations* (Addison-Wesley, Reading, Mass., 1968), p. 64.
18. L. W. Casperson and A. Yariv, "The Gaussian Mode in Optical Resonators with a Radial Gain Profile," Appl. Phys. Lett. **12,** 355 (1968).
19. J. T. Verdeyen, *Laser Electronics* (Prentice-Hall, Englewood Cliffs, N.J., 1981), Chap. 1.
20. P. Rossi, C. W. McCurdy, and R. L. McCreery, "Diffractive Spectroelectrochemistry. Use of Diffracted Light for Monitoring Electrogenerated Chromophores," J. Am. Chem. Soc. **103,** 2524 (1981).
21. R. Pruiksma and R. L. McCreery, "Observation of Electrochemical Concentration Profiles by Absorption Spectroelectrochemistry," Anal. Chem. **51,** 2253 (1979).
22. J. T. Knudtson and K. L. Ratzlaff, "Laser Beam Spatial Profile Analysis Using a Two-Dimensional Photodiode Array," Rev. Sci. Instrum. **54,** 856 (1983).